Dissipative Phase Transition with Driving-Controlled Spatial Dimension and Diffusive Boundary Conditions

Zejian Li,[1,*] Ferdinand Claude,[2,*] Thomas Boulier,[2] Elisabeth Giacobino,[2] Quentin Glorieux,[2] Alberto Bramati,[2] and Cristiano Ciuti[1]

[1]*Laboratoire Matériaux et Phénomènes Quantiques (MPQ), Université de Paris, CNRS-UMR7162, Paris 75013, France*
[2]*Laboratoire Kastler Brossel, Sorbonne Université, CNRS, ENS-Université PSL, Collège de France, Paris 75005, France*

(Received 19 October 2021; accepted 1 February 2022; published 28 February 2022)

We investigate theoretically and experimentally a first-order dissipative phase transition, with diffusive boundary conditions and the ability to tune the spatial dimension of the system. The considered physical system is a planar semiconductor microcavity in the strong light-matter coupling regime, where polariton excitations are injected by a quasiresonant optical driving field. The spatial dimension of the system from 1D to 2D is tuned by designing the intensity profile of the driving field. We investigate the emergence of criticality by increasing the spatial size of the driven region. The system is nonlinear due to polariton-polariton interactions and the boundary conditions are diffusive because the polaritons can freely diffuse out of the driven region. We show that no phase transition occurs using a 1D driving geometry, while for a 2D geometry we do observe both in theory and experiments the emergence of a first-order phase transition. The demonstrated technique allows all-optical and *in situ* control of the system geometry, providing a versatile platform for exploring the many-body physics of photons.

DOI: 10.1103/PhysRevLett.128.093601

Introduction.—The study of phase transitions and critical phenomena is at the heart of condensed matter physics and material science [1]. In classical systems, thermal phase transitions, such as that from a liquid to a solid phase, occur at finite temperature and are driven by thermal fluctuations. In a closed quantum system, phase transitions can happen at zero temperature, where the system is in its ground state, driven by quantum fluctuations due to the competition of noncommuting terms in the Hamiltonian [2]. On the other hand, open quantum systems subject to driving and dissipation can exhibit dissipative phase transitions for the nonequilibrium steady state, where the physics is decided by the rich interplay between the Hamiltonian evolution, dissipation-induced fluctuations, and driving.

Driven-dissipative phase transitions have been theoretically studied for various systems, such as photonic resonators [3–16], exciton-polariton condensates [17–20], and spin systems [21–28]. Experimental investigations have studied dissipative phase transitions in single-mode semiconductor microcavity pillars [29] and superconducting resonators [30,31]. Recent theoretical works [11,16] predicted that in a driven-dissipative lattice of photonic resonators with Kerr nonlinearities a first-order dissipative phase transition emerges in two-dimensional (2D) lattices (with periodic boundary conditions), while in 1D chains there is no critical phenomenon. Note that in general the emergence of a phase transition can be drastically affected by its spatial dimensionality [2].

In this work, we explore both theoretically and experimentally the role of spatial dimension for a dissipative phase transition using a planar semiconductor microcavity, where polariton excitations are injected via quasiresonant driving. We propose theoretically and implement experimentally an all-optical way to enforce the dimensionality via the spatial shape of the driving beam. In particular, we consider a top-hat spot with constant driving intensity. The shape of the spot can be tailored *in situ* to create a 2D or 1D geometry [32]. This scheme also features "diffusive" boundary conditions, since the polaritons can diffuse away from the driven region. While increasing the spatial size of the spot, which is the thermodynamic limit in the present context, we show that a first-order phase transition occurs using a 2D geometry, while it disappears in the 1D configuration, providing a first experimental demonstration of the role of dimensionality in driven-dissipative phase transitions of photonic systems.

Theoretical model.—Consider a planar semiconductor microcavity in the strong light-matter coupling regime, where polariton excitations are coherently injected by a quasiresonant optical drive. The system dynamics can be described in terms of the lower polariton field $\hat{\psi}(\mathbf{r}, t)$ [33], where $\mathbf{r} = (x, y)$ are in-plane coordinates parallel to the cavity mirrors. Within the mean-field approximation [34], the time evolution of the mean field $\psi(\mathbf{r}, t) = \langle \hat{\psi}(\mathbf{r}, t) \rangle$ in the frame rotating at the driving frequency ω_d can be described by the dynamical equation [33]:

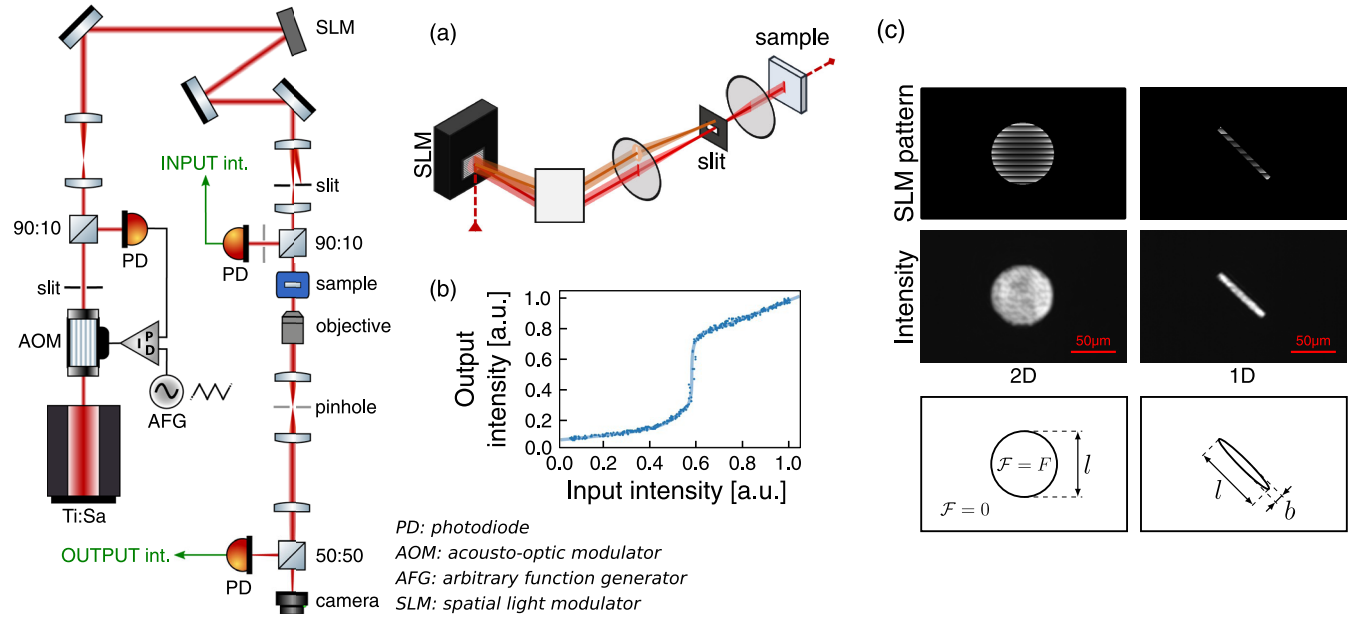

FIG. 1. Sketch of the experimental setup. The laser is slaved using a proportional-integral-derivative (PID) controller, an arbitrary function generator (AFG) and an acousto-optic modulator loop to produce a power ramp; its intensity profile is reshaped using a spatial light modulator. Two photodiodes (PD) measure the power inside disks of diameter $l_D = 5$ μm at the center of the beams at the sample input and output. (a) Pump intensity profile shaping method: the light (dark) beam represents the zero (first) order of the diffracted beam from the SLM. (b) Output intensity from the sample as a function of the input intensity, plotted for a pump detuning of $\Delta = \gamma$ and a 2D top-hat drive of diameter $l = 30$ μm. (c) SLM phase pattern (upper) for obtaining 2D (left) and 1D (right) flat-top beam profiles (middle) of different sizes and intensities (bottom).

$$i\frac{\partial}{\partial t}\psi(\mathbf{r},t) = \left(-\Delta - \frac{\hbar}{2m}\nabla^2\right)\psi(\mathbf{r},t) + g|\psi(\mathbf{r},t)|^2\psi(\mathbf{r},t) - i\frac{\gamma}{2}\psi(\mathbf{r},t) + \mathcal{F}(\mathbf{r}), \quad (1)$$

where $\hbar$ is the Planck constant, $\Delta = \omega_d - \omega_{\mathrm{LP}}^{k=0}$ is the detuning of the drive with respect to the $k = 0$ mode of the lower polariton branch, m is the lower polariton effective mass, g is the polariton-polariton interaction constant, γ is the lower polariton loss rate, and $\mathcal{F}(\mathbf{r})$ encodes the amplitude and spatial shape of the coherent drive.

In the following, we adopt a top-hat driving scheme [see Fig. 1(c)], where the amplitude $\mathcal{F}(\mathbf{r})$ is defined by

$$\mathcal{F}(\mathbf{r}) = F\mathbb{1}_A(\mathbf{r}), \quad (2)$$

where $\mathbb{1}_A$ is the indicator function of a compact region A of the plane, such that the drive is constant within the region A and zero elsewhere. To force a 1D geometry, the driving region will be chosen as an elliptical spot with fixed minor axis b and variable major axis $l \gg b$. To induce a 2D geometry, instead, the driving region will be chosen as a circular disk of variable diameter l. Note that the only difference between the 1D and 2D configurations is the spatial shape of the top-hat drive [38], while the planar microcavity sample is the same. The boundary conditions in terms of the driven region are therefore of diffusive nature, which means that the polaritons can freely diffuse and decay out of the driving spot.

In order to probe a dissipative phase transition with respect to the driving intensity $I = |F|^2$, we will be interested in the steady-state polariton density averaged over a disk D of diameter l_D at the center of the driven region:

$$n_D^{\mathrm{SS}} = \frac{1}{\mu(D)}\int_D \mathrm{d}^2\mathbf{r}|\psi_{\mathrm{SS}}(\mathbf{r})|^2, \quad (3)$$

where $\mu(D)$ denotes the area of the disk D and ψ_{SS} is the steady-state field such that $\partial_t\psi_{\mathrm{SS}} = 0$. In the thermodynamic limit of $l \to \infty$, a transition between two phases is characterized by the nonanalytical behavior of n_D^{SS} when I tends to some critical value I_c. Formally, a transition of order M can be described as [39]

$$\lim_{I\to I_c}\left|\frac{\partial^M}{\partial I^M}\lim_{l\to\infty} n_D^{\mathrm{SS}}\right| = +\infty. \quad (4)$$

In this Letter we will present a first order ($M = 1$) phase transition, that is a discontinuity of steady-state polariton density n_D^{SS} with respect to the drive intensity I, which are the two quantities that we measure in our experiments.

Experimental setup.—The sample used in our experiments is a 2λ GaAs high-finesse semiconductor

microcavity cooled to the temperature of 4 K in an open-flow helium cryostat. The cavity embeds three $In_{0.04}Ga_{0.96}As$ quantum wells (QWs) between a pair of distributed Bragg mirrors made of 21 (top) and 24 (bottom) alternated layers of GaAs/AlAs. Each QW is located on an antinode of the cavity electromagnetic field to have a strong coupling of QW excitons to the cavity photons, giving rise to the exciton-polariton modes. The cavity spacer has a small wedge ($\hbar w \simeq 0.7\ \mu\mathrm{eV}/\mu\mathrm{m}$) whereby the photon-exciton detuning can be finely adjusted to around 0 meV by changing the excitation position. At this detuning the lower polariton branch has an effective mass $m = 5.7 \times 10^{-5} m_e$, where m_e is the bare electron mass. The Rabi frequency, the lower-polariton decay rate, and the polariton-polariton interaction constant are, respectively, measured to be $\hbar\Omega_R = 5.1$ meV, $\hbar\gamma = 0.08$ meV, and $\hbar g = 0.01\ \mathrm{meV} \cdot\ \mu\mathrm{m}^2$ [40].

The polaritons are excited by a circularly polarized continuous-wave Ti:sapphire laser whose output Gaussian mode is reshaped with a spatial light modulator (SLM) (Fig. 1). The SLM liquid crystal matrix plane is imaged on that of the cavity and contains a blazed grating of tunable contrast, which diffracts in the first order a fraction of the driving field intensity. The first order component is sent at normal incidence through the cavity, while the non-diffracted part (zero order) is blocked in the Fourier plane with a slit [Fig. 1(a)].

By locally adjusting the grating contrast, we modify the intensity distribution between the zero and the first orders. In this way, with a well-calibrated anti-Gaussian contrast gradient—minimum at the center and maximum at the edge of the spot—we produce in the first order a flat top-hat intensity profile. Then, by adding a non-diffracting mask over the grating, one can select which area of the beam profile is reflected into the first order. Thus, the shape of the driving spot in the cavity reproduces the one defined by the contours of the mask [Fig. 1(c)]. With this reshaping method, we can go from a 2D circular driving spot to a 1D elliptical one, by configuring the SLM respectively with a blazed grating masked by a circular aperture or by a narrow slit (see Fig. 1). In the following, the spot sizes in the cavity plane are tuned by changing the mask dimension. For the 1D geometry, the minor axis of the intensity profile is set at $b = 6.4\ \mu$m [41].

In order to probe the phase transition, an acousto-optic modulator (AOM) modulates the driving field power with a low-frequency ramp (200 Hz) of sufficient amplitude to be able to scan a wide range of polariton density. The input and output intensities of the cavity are measured using two photodiodes which detect through pinholes (of diameter $l_D = 5\ \mu$m [42]) at the center of the driving spot. Thus, the polariton density is directly observed as a function of the driving intensity by plotting, one with respect to the other, the powers detected by the two photodiodes [see Fig. 1(b)].

Results and discussion.—To investigate the steady-state behavior of the system and probe the phase transition, we solved Eq. (1) numerically with the experimental parameters introduced in the previous section [43] and the detuning is set to $\Delta = \gamma$ in the simulation (same value as in the experiments), which is in the regime where a driven-dissipative Kerr cavity exhibits mean-field bistability [29,44]. This can be equivalently viewed as the approximation of considering only the $k = 0$ mode under uniform drive F [9], since the steady-state mean-field equation can be written as

$$|\psi_{\mathrm{SS}}|^2\left[(\Delta - g|\psi_{\mathrm{SS}}|^2)^2 + \frac{\gamma^2}{4}\right] = |F|^2. \tag{5}$$

Note that the nonlinear relation between $|\psi_{\mathrm{SS}}|^2$ and $I = |F|^2$ predicts a bistable regime if $\Delta/\gamma > \sqrt{3}/2$, as shown by the dashed line in Fig. 2(d), that we will compare with our numerical results. In all the simulations, the diameter of the probing disk D is set to $l_D = 5\ \mu$m and in the 1D configuration the minor-axis of the driving spot is $b = 6.4\ \mu$m, which are also the values adopted in our experiments.

In Figs. 2(a)–2(c) [2(d)–2(f)] we present our theoretical and experimental results for the 1D [2D] driving geometry. In both configurations, the steady-state polariton density n_D^{SS} averaged over the probing disk increases as a function of the driving intensity I and the maximum slope $\mathcal{S}(l) = \max_I\{[\partial n_D^{\mathrm{SS}}(I,l)]/\partial I\}$ of the crossover from low density to high density (obtained with a noise-robust numerical differentiation method [45]) is monitored as a function of the top-hat size l, which allows us to probe the emergence of phase transitions defined by Eq. (4). In the 1D configuration, where the top-hat drive takes the shape of an elliptical spot with fixed minor axis, the slope $\mathcal{S}(l)$ saturates to a finite value with low enhancement [$\mathcal{S}(l)/\mathcal{S}(l_0) < 2$ with $l_0 = 15\ \mu$m for all values of l measured] as the major axis l increases, signifying a smooth crossover with no phase transition in the thermodynamic limit.

In sharp contrast to the 1D configuration, with a 2D driving geometry, the slope presents a significant enhancement (by a factor of around 40 in theory, and a comparable value in the experimental results) as the top-hat diameter l increases, suggesting the emergence of a first-order phase transition in the thermodynamic limit of $l \to \infty$. We would like to also point out that, while in the 1D configuration we observed no bistability, in the experiments with 2D geometry we observed slight bistability for top-hat diameters $l \gtrsim 35\ \mu$m [in this case we consistently took the lower branch when computing the slope (the higher one would give similar results)], which is consistent with the critical slowing down [34] of the dynamics as the system approaches criticality in two dimensions. Note that for $\mathcal{S}(l)/\mathcal{S}(l_0) \gtrsim 10$ [corresponding to a top-hat size of $l \gtrsim 30$

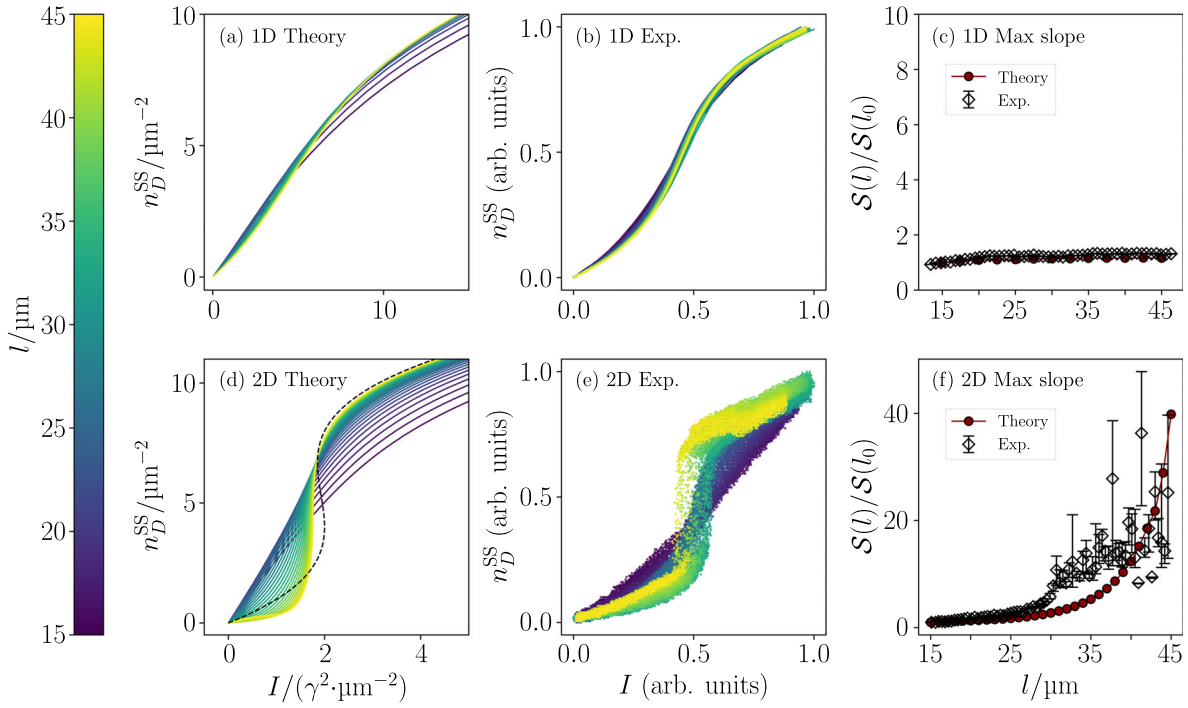

FIG. 2. (a) [(b)] Theoretical (experimental) results for the steady-state polariton density n_D^{SS} averaged over the probing disk as a function of the drive intensity I for different top-hat spot sizes l (see color bar) in the 1D configuration with detuning $\Delta = \gamma$. (c) The maximum derivative $\mathcal{S}(l)$ for each top-hat size l normalized by the maximum derivative at $l_0 = 15$ μm, for both theoretical and experimental results (see legend). (d)–(f) The same quantities as in (a)–(c) for the 2D configuration. The dashed line in (d) is the prediction of the mean-field theory in Eq. (5). Note that as the top hat increases in size, the slope in the 1D configuration quickly saturates for increasing size l, while in the 2D configuration the slope sharply increases in both theory and experiment, as expected for a first order phase transition.

in the experimental results in Fig. 2(e)], the curve becomes almost vertical [$\tan^{-1}(10) \simeq 84°$], which makes the numerically computed derivatives more sensitive to small errors in the measurements, resulting in the relatively larger error bars on the experimental curve in Fig. 2(f) in this regime [46].

Conclusion and outlook.—In this work, we have demonstrated both experimentally and theoretically the emergence of a first-order dissipative phase transition of polaritons in a planar microcavity subjected to a top-hat driving scheme with naturally diffusive boundary conditions. We have shown that the emergence of criticality in such photonic system with Kerr nonlinearity is determined by the spatial dimension via the geometry imposed by the top-hat driving spot: a 1D geometry leads to a crossover behavior with no phase transition, while a 2D geometry shows a behavior consistent with a first-order transition between two phases with different densities, which, to the best of our knowledge, is the first experimental demonstration of the role of dimensionality in determining criticality in driven-dissipative photonic systems.

The approach presented in this work allows the study of both 1D and 2D problems using the same planar cavity. The ability to control the criticality of the system via the spatial profile of the drive can also bring new insights to the design of polaritonic devices such as all-optical polariton transistors [47]. This scheme can be potentially generalized to more complicated geometries imprinted by the shape of the driving field, such as fractal patterns or quasiperiodic lattices, which could open the possibilities for studying effects of gradual changes of the dimensionality on phase transitions, paving the way to a novel approach to exploring the many-body physics of photons and critical phenomena.

We would like to acknowledge discussions with Z. Denis. This work was supported by the FET FLAGSHIP Project PhoQuS (Grant Agreement ID: 820392) and by Project NOMOS (ANR-18-CE24-0026). This work was granted access to the HPC resources of TGCC under the allocation A0100512462 attributed by GENCI (Grand Equipement National de Calcul Intensif). A. B. and Q. G. are members of the Institut Universitaire de France (IUF).

[*] These authors contributed equally to this work.

[1] H. E. Stanley, *Introduction to Phase Transitions and Critical Phenomena* (Oxford University Press, Oxford, 1987).
[2] S. Sachdev, *Quantum Phase Transitions* (Cambridge University Press, Cambridge, England, 2009).

[3] N. Bartolo, F. Minganti, W. Casteels, and C. Ciuti, Exact steady state of a Kerr resonator with one- and two-photon driving and dissipation: Controllable Wigner-function multimodality and dissipative phase transitions, Phys. Rev. A **94**, 033841 (2016).
[4] H. J. Carmichael, Breakdown of Photon Blockade: A Dissipative Quantum Phase Transition in Zero Dimensions, Phys. Rev. X **5**, 031028 (2015).
[5] H. Weimer, Variational Principle for Steady States of Dissipative Quantum Many-Body Systems, Phys. Rev. Lett. **114**, 040402 (2015).
[6] M. Benito, C. S. Muñoz, and C. Navarrete-Benlloch, Degenerate parametric oscillation in quantum membrane optomechanics, Phys. Rev. A **93**, 023846 (2016).
[7] J. J. Mendoza-Arenas, S. R. Clark, S. Felicetti, G. Romero, E. Solano, D. G. Angelakis, and D. Jaksch, Beyond mean-field bistability in driven-dissipative lattices: Bunching-antibunching transition and quantum simulation, Phys. Rev. A **93**, 023821 (2016).
[8] W. Casteels, F. Storme, A. Le Boité, and C. Ciuti, Power laws in the dynamic hysteresis of quantum nonlinear photonic resonators, Phys. Rev. A **93**, 033824 (2016).
[9] W. Casteels, R. Fazio, and C. Ciuti, Critical dynamical properties of a first-order dissipative phase transition, Phys. Rev. A **95**, 012128 (2017).
[10] W. Casteels and C. Ciuti, Quantum entanglement in the spatial-symmetry-breaking phase transition of a driven-dissipative Bose-Hubbard dimer, Phys. Rev. A **95**, 013812 (2017).
[11] M. Foss-Feig, P. Niroula, J. T. Young, M. Hafezi, A. V. Gorshkov, R. M. Wilson, and M. F. Maghrebi, Emergent equilibrium in many-body optical bistability, Phys. Rev. A **95**, 043826 (2017).
[12] M. Biondi, G. Blatter, H. E. Türeci, and S. Schmidt, Nonequilibrium gas-liquid transition in the driven-dissipative photonic lattice, Phys. Rev. A **96**, 043809 (2017).
[13] A. Biella, F. Storme, J. Lebreuilly, D. Rossini, R. Fazio, I. Carusotto, and C. Ciuti, Phase diagram of incoherently driven strongly correlated photonic lattices, Phys. Rev. A **96**, 023839 (2017).
[14] V. Savona, Spontaneous symmetry breaking in a quadratically driven nonlinear photonic lattice, Phys. Rev. A **96**, 033826 (2017).
[15] W. Verstraelen, R. Rota, V. Savona, and M. Wouters, Gaussian trajectory approach to dissipative phase transitions: The case of quadratically driven photonic lattices, Phys. Rev. Research **2**, 022037(R) (2020).
[16] F. Vicentini, F. Minganti, R. Rota, G. Orso, and C. Ciuti, Critical slowing down in driven-dissipative Bose-Hubbard lattices, Phys. Rev. A **97**, 013853 (2018).
[17] L. M. Sieberer, S. D. Huber, E. Altman, and S. Diehl, Dynamical Critical Phenomena in Driven-Dissipative Systems, Phys. Rev. Lett. **110**, 195301 (2013).
[18] L. M. Sieberer, S. D. Huber, E. Altman, and S. Diehl, Nonequilibrium functional renormalization for driven-dissipative Bose-Einstein condensation, Phys. Rev. B **89**, 134310 (2014).
[19] E. Altman, L. M. Sieberer, L. Chen, S. Diehl, and J. Toner, Two-Dimensional Superfluidity of Exciton Polaritons Requires Strong Anisotropy, Phys. Rev. X **5**, 011017 (2015).
[20] G. Dagvadorj, M. Kulczykowski, M. H. Szymańska, and M. Matuszewski, First-order dissipative phase transition in an exciton-polariton condensate, Phys. Rev. B **104**, 165301 (2021).
[21] T. E. Lee, S. Gopalakrishnan, and M. D. Lukin, Unconventional Magnetism via Optical Pumping of Interacting Spin Systems, Phys. Rev. Lett. **110**, 257204 (2013).
[22] J. Jin, A. Biella, O. Viyuela, L. Mazza, J. Keeling, R. Fazio, and D. Rossini, Cluster Mean-Field Approach to the Steady-State Phase Diagram of Dissipative Spin Systems, Phys. Rev. X **6**, 031011 (2016).
[23] E. M. Kessler, G. Giedke, A. Imamoglu, S. F. Yelin, M. D. Lukin, and J. I. Cirac, Dissipative phase transition in a central spin system, Phys. Rev. A **86**, 012116 (2012).
[24] T. E. Lee, H. Häffner, and M. C. Cross, Antiferromagnetic phase transition in a nonequilibrium lattice of Rydberg atoms, Phys. Rev. A **84**, 031402 (2011).
[25] C.-K. Chan, T. E. Lee, and S. Gopalakrishnan, Limit-cycle phase in driven-dissipative spin systems, Phys. Rev. A **91**, 051601(R) (2015).
[26] R. Rota, F. Storme, N. Bartolo, R. Fazio, and C. Ciuti, Critical behavior of dissipative two-dimensional spin lattices, Phys. Rev. B **95**, 134431 (2017).
[27] V. R. Overbeck, M. F. Maghrebi, A. V. Gorshkov, and H. Weimer, Multicritical behavior in dissipative Ising models, Phys. Rev. A **95**, 042133 (2017).
[28] D. Roscher, S. Diehl, and M. Buchhold, Phenomenology of first-order dark-state phase transitions, Phys. Rev. A **98**, 062117 (2018).
[29] S. R. K. Rodriguez, W. Casteels, F. Storme, N. C. Zambon, I. Sagnes, L. Le Gratiet, E. Galopin, A. Lemaître, A. Amo, C. Ciuti, and J. Bloch, Probing a Dissipative Phase Transition via Dynamical Optical Hysteresis, Phys. Rev. Lett. **118**, 247402 (2017).
[30] T. Fink, A. Schade, S. Höfling, C. Schneider, and A. Imamoglu, Signatures of a dissipative phase transition in photon correlation measurements, Nat. Phys. **14**, 365 (2018).
[31] M. Fitzpatrick, N. M. Sundaresan, A. C. Y. Li, J. Koch, and A. A. Houck, Observation of a Dissipative Phase Transition in a One-Dimensional Circuit QED Lattice, Phys. Rev. X **7**, 011016 (2017).
[32] In principle, one could also use etching techniques, that may lead to better defined structures, to study the effect of spatial dimension on dissipative phase transitions. However, the present all-optical approach provides flexibility and can be used to explore the effect of a gradual change of dimensionality *in situ* using the same sample.
[33] I. Carusotto and C. Ciuti, Quantum fluids of light, Rev. Mod. Phys. **85**, 299 (2013).
[34] See Supplemental Material at http://link.aps.org/supplemental/10.1103/PhysRevLett.128.093601 for a derivation of the mean-field dynamics from the quantum master equation [35], for a benchmark against the truncated Wigner method [36,37], as a justification of this approximation, and for a discussion on the critical slowing down based on our numerical simulations.

[35] H.-P. Breuer and F. Petruccione, *The Theory of Open Quantum Systems* (Oxford University Press, New York, 2007).

[36] K. Vogel and H. Risken, Quasiprobability distributions in dispersive optical bistability, Phys. Rev. A **39**, 4675 (1989).

[37] H. J. Carmichael, *Statistical Methods in Quantum Optics 1* (Springer, Berlin, Heidelberg, 1999).

[38] Note that the way we distinguish 1D and 2D is not via the absolute size of the top-hat spot, but the different ways they approach the thermodynamic limit: In one dimension only the major axis l increases with b fixed, such that in the thermodynamic limit $\lim_{l\to\infty} b/l = 0$, whereas in two dimensions both axes increase at the same rate, keeping the spot always circular and its aspect ratio constant.

[39] F. Minganti, A. Biella, N. Bartolo, and C. Ciuti, Spectral theory of Liouvillians for dissipative phase transitions, Phys. Rev. A **98**, 042118 (2018).

[40] As we will choose a detuning of $\Delta = \gamma$ with respect to the lower polariton branch in the next section, this means that the Rabi frequency $\hbar\Omega_R$, which determines the minimum splitting between the lower and upper polariton branches, is much larger than all the other energy scales in the problem. We can therefore consider effectively only the lower polariton in our theoretical treatment [33].

[41] This value is chosen such that it is large compared to the optical wavelength of the laser to avoid undesirable diffraction effects so as to produce a well-defined top hat. At the same time, it should be small enough to ensure that the crossover slope for the smallest top hat is mild enough to be measured experimentally, which allows us to study the asymptotic behavior (convergence or divergence) of the growing slope.

[42] Note that as the probing disk D is placed concentrically with the top-hat profile, the chosen value ensures that it is always contained within the driven region. However, we expect that asymptotically (in the limit of large l), the observed effects should not depend on its specific position as long as the probing disk is far enough from the boundary (or the edges of the major axis in the 1D case) of the top hat.

[43] Throughout the simulation results presented in this section, the cavity wedge is not taken into account for more efficient simulations. See Supplemental Material [34] for more technical details on the simulation and the effect of the cavity wedge.

[44] A. Baas, J.-Ph. Karr, M. Romanelli, A. Bramati, and E. Giacobino, Optical bistability in semiconductor microcavities in the nondegenerate parametric oscillation regime: Analogy with the optical parametric oscillator, Phys. Rev. B **70**, 161307(R) (2004).

[45] R. Chartrand, Numerical differentiation of noisy, nonsmooth data, ISRN Appl. Math. **2011**, 1 (2011).

[46] The deviation between the theoretical and the experimental curves could originate from a slightly higher detuning in the experiment than the nominal value $\Delta = \gamma$. Nevertheless, the main objective of this plot is to show the divergence in the 2D configuration for both theory and experiment, which is in clear contrast to the 1D case.

[47] D. Ballarini, M. De Giorgi, E. Cancellieri, R. Houdré, E. Giacobino, R. Cingolani, A. Bramati, G. Gigli, and D. Sanvitto, All-optical polariton transistor, Nat. Commun. **4**, 1778 (2013).